RBF-based aerodynamic optimization of an industrial glider

Emiliano Costa

D'Appolonia SpA

Rome, Italy

Marco E. Biancolini, Corrado Groth

University of Rome Tor Vergata

Rome, Italy

Ubaldo Cella

Design Methods™ (www.designmethods.aero)

Messina, Italy

Gregor Veble., Matej Andrejasic

Pipistrel d.o.o.

Ajdovščina, Slovenia

Corresponding Author: emiliano.costa@dappolonia.it

Summary

The present paper is addressed to the improvement of the aerodynamic design of an industrial glider flying at Mach 0.08. The original design exhibits performance affecting separation occurring in the wing-fuselage junction region at high incidence angles. Adopting a numerical optimization approach affordable in the case that HPC resources are limited, the separation was significantly reduced updating the local geometry of fuselage and fairing maintaining the wing airfoil unchanged. Shape variations were applied to the glider's baseline configuration through a mesh morphing technique founded on the mathematical framework of radial basis functions (RBFs). The computational outputs were obtained employing a combined use of ANSYS® DesignXplorer™, ANSYS® Fluent® and RBF Morph™ software working in the ANSYS® Workbench™ environment. The k-ω SST turbulence model was used with two levels of structured hexahedral meshes, both generated using ANSYS® ICEM CFD™: a coarse grid to be used applying wall functions and a fine version with cells clustering aimed to solve the boundary layer up to the wall. The coarse mesh allows to quickly tune and set-up the overall workflow keeping the high fidelity one for the final optimisation run. Two shape modifiers were set up by means of RBF Morph™ to drive shape morphing guaranteeing, at the same time, the fulfilment of the manufacturing constraints. Once the RBF solutions were computed and made available, a DoE optimization calculation was set up using ANSYS® DesignXplorer™ and, after performing CFD runs through ANSYS® Fluent®, the potential optimal candidates maximizing the aerodynamic efficiency were identified by means of the response surface approach. A relevant aerodynamic efficiency improvement was finally gained moulding the glider's geometry according to the selected optimal design point. Such an optimization study is part of an explorative set of analyses that focused on better addressing the numerical strategies to be employed in the development of the EU FP7 Project RBF4AERO.

1 Introduction

Taurus glider, designed and manufactured by Pipistrel d.o.o. Ajdovščina Slovenia (Figure 1 and Figure 2), is a side-by-side two-seat self-launching ultra-light glider made out of composite materials. The wing is located in a vertical central position respect to the fuselage, whilst its longitudinal position is aft the maximum section, behind the cockpit, in a significant positive pressure gradient.

Figure 1. Taurus glider

This configuration implies that, in the fuselage junction region, the wing suffers an extra increase of flow velocity close to the leading edge and a significant adverse pressure gradient in the trailing edge region that cause a leading edge separation at high angles of attach (AoA). The problem is particularly felt when

lowering the Reynolds number (increasing the altitude) effecting a falling of the overall aircraft aerodynamic efficiency in manoeuvring.

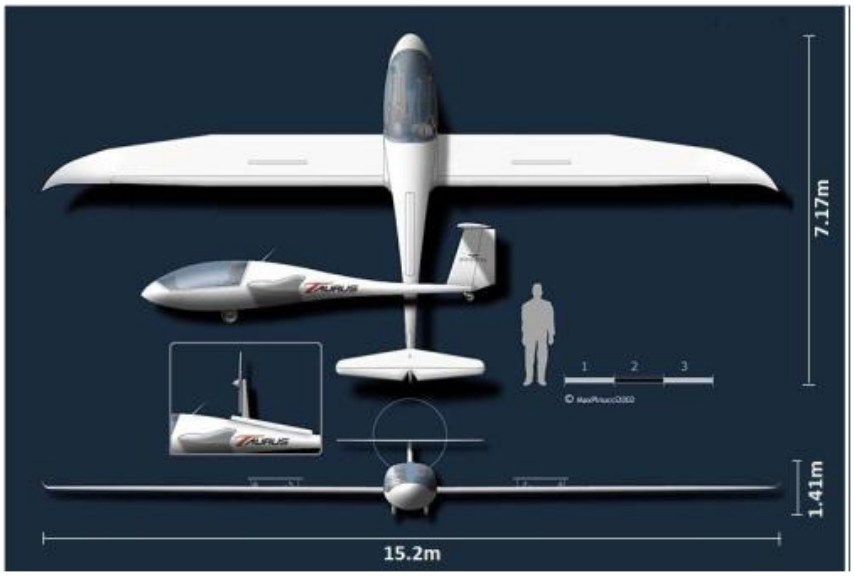

Figure 2. Taurus orthographic representation

The occurrence of separated flow conditions was demonstrated experimentally by performing flight tests (Figure 3). The flow attachment on glider's shape was monitored by means of small rectangular pieces of adhesive tape - tufts. Unordered direction of tufts at the wing/fuselage fairing clearly indicates a detached flow that is propagating according to a delta shape in the streamwise direction.

The main objective of the present work is to apply a shape optimization numerical procedure based on mesh morphing in order to diminish such a separation region and consequently enhance the aerodynamic efficiency of the glider.

Figure 3. Snapshot of the instant at which the flow detachment occurs

Another objective of this study is to show how the glider can be aerodynamically optimized using a low-demanding computational approach to develop the optimization analysis, limiting the utilization of the high-demanding computational model to confirm and deepen the numerical results.

This study is part of a set of explorative analyses that aimed at anticipating the investigation of the proper shape modifications to be applied in view of carrying out the scheduled computational applications of the RBF4AERO Project [R1].

2 Shape optimization through RBF mesh morphing technique

RBFs are a class of mathematical interpolation functions that, in computer-aided engineering (CAE) applications, can be used to drive mesh morphing (smoothing) of the discretized domain of the computational model applying predefined displacements to a set of purposely generated points, called source points. As example, Figure 4 depicts the localization of source nodes of the study deepened hereafter.

The main characteristics of such an approach are the meshless property, the preservation of mesh consistency and the low disk usage in addition to standard calculation, whilst some among its main advantages are the exact control of nodes during smoothing, the prevention of remeshing noise, the possibility to be fully integrated in the computing process and the high performance in handling large models.

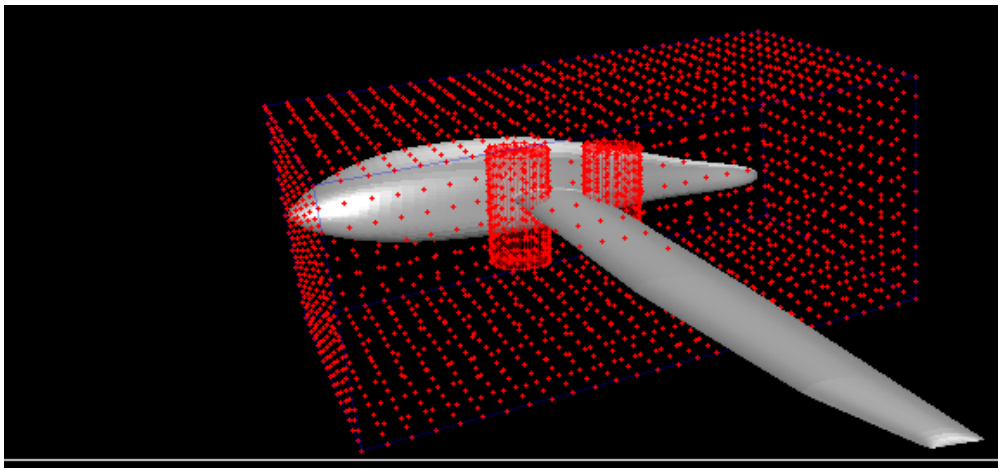

Figure 4. Source nodes' position before applying morphing

The RBF mesh morphing technique is the core of the RBF4AERO Project which aims at developing the RBF4AERO Benchmark Technology, an integrated numerical platform and methodology to efficiently face the most demanding challenges of aircrafts design and optimization [R1]. This project represents the great occasion to further push and extend the application of mesh morphing in the aviation sector after it received lots of acknowledgments in other industrial field such as automotive [R2], motorsport [R3] [R4], naval [R5] and medical [R6]. In particular, the intent of RBF4AERO is to cover modern aeronautical design applications such as shape optimization [R7], ice accretion simulation [R8], fluid-structure interaction (FSI)[R9][R10], adjoint-morphing coupling and multi-physics optimization analyses through efficient procedures based on RBF mesh morphing such to prevent the typical compromise of standard optimization procedures in terms of speed, accuracy and extent.

3 Outline of the proposed numerical optimization process

The workflow of the optimization procedure proposed in the present work is illustrated in Figure 5 through a block diagram and according to its most general framework. In that representation, rectangular blocks

represent computational data, circular blocks identify specific operations or features, whilst blocks dealing with the use of the same tool are included in a coloured region.

That workflow, totally manageable in the ANSYS® Workbench™ (WB) environment, foresees the availability of the computer-aided design (CAD) representing the baseline configuration of the model to be studied, and provides, as final output, the CAD of the optimized shapes of such a model. In particular, the operations characterised by the highest level of automation are those performed by means of ANSYS® DesignXplorer™ (DX) which acts as driver of the entire optimization procedure and whose functioning needs the computational fluid dynamics (CFD) model of the baseline configuration (see paragraph 4.1) as well as the access to stored RBF solutions (see paragraph 4.2).

DX supports the sequential accomplishment of the main phases of optimization. Specifically, the first one envisages the partial populating of the design of experiment (DoE) table having a number of rows and columns respectively equal to the number of design points (DPs) and the summation of shape variations and objective functions (aerodynamic coefficients and efficiency). The filled portion concerns the combinations of RBF solutions' amplification values, whereas the unfilled portion (blank columns) waits for the computing of the objective functions. Successively, once a CFD simulation is ran for each DP (DoE analysis), the DoE table is completed and its data can thus be processed and visualized through the response surface method (RSM). At this point, the optimization can be completed with the purpose to identify the optimal combination of RBF solutions that, applied to the baseline CFD model and starting CAD, generates the optimal CFD model and CAD configuration respectively (see section 5).

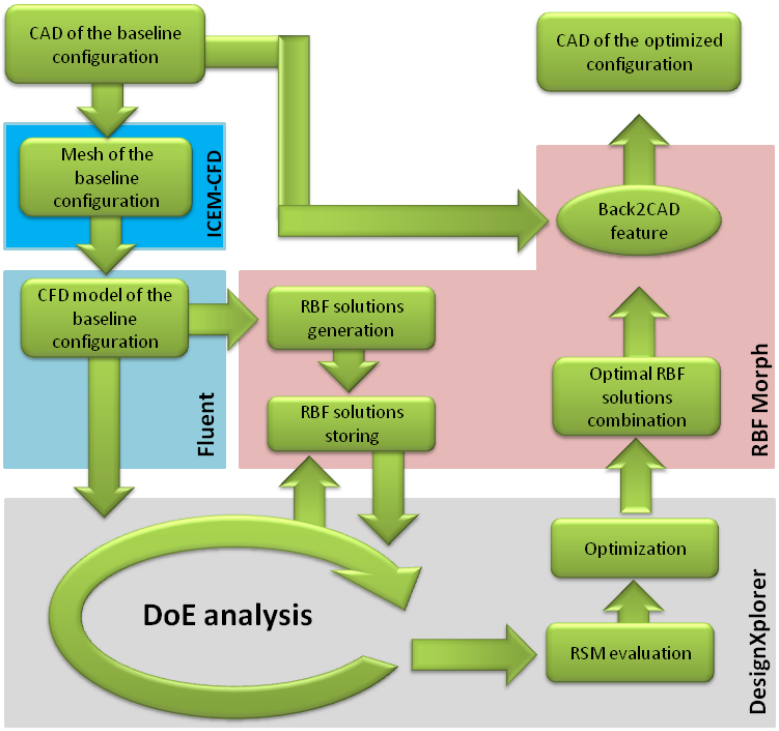

Figure 5. Workflow of the mesh morphing based shape optimization procedure in the ANSYS® Workbench™ environment

It is worth to mention that the optimal solution identification can be carried out in different fashions because of several reasons such as specific design needs, adopted optimization strategy or final accuracy, whilst the CAD of the optimized configuration is finally obtained by morphing the starting CAD through the back2CAD feature of RBF Morph.

4 CFD results of the baseline model and RBF solutions generation

4.1 CFD results of the baseline model

The model of the glider was provided by Pipistrel. In order to reduce the computational effort it consists of a simplified version of the real aircraft in which only the areas of interest are accurately reproduced (winglets and tail are not modelled).

As already anticipated, two computational domains were generated: a coarse grid to conduct optimization and a fine one to be employed to verify, at a higher level of accuracy, the quality of the solutions obtained. Exploiting the symmetry of the flow field, both meshes model just half domain. Those grids are multi-block structured hexahedral and are extended around 40 wing chords upstream the model, 60 downstream and 50 on the side. The dimensions are 1.4 million of cells for the coarse grid and 7 million for the fine one. The Figure 6 details the cells distribution for the two meshes on wall surfaces.

The CFD study of the baseline configuration for both computational models was ran through Fluent adopting the same set-up foreseeing 8° for the AoA, a flow regime characterized by a Mach number of 0.08 with a $1.24 \bullet 10^6$ Reynolds number based on reference chord of length 0.8 m, and with physical properties values dictated by the atmospheric conditions at 2000 metres of altitude. Given the subsonic condition of the problem, air was considered as incompressible whilst the k-ω SST turbulence model was applied. Relating to boundary conditions, velocity inlet and pressure outlet boundary condition were respectively imposed to the inlet and outlet surface of the box-shaped simulation volume, a symmetry condition to the surface of symmetry, a no-slip condition to glider's surfaces and a wall free slip condition on remaining surfaces.

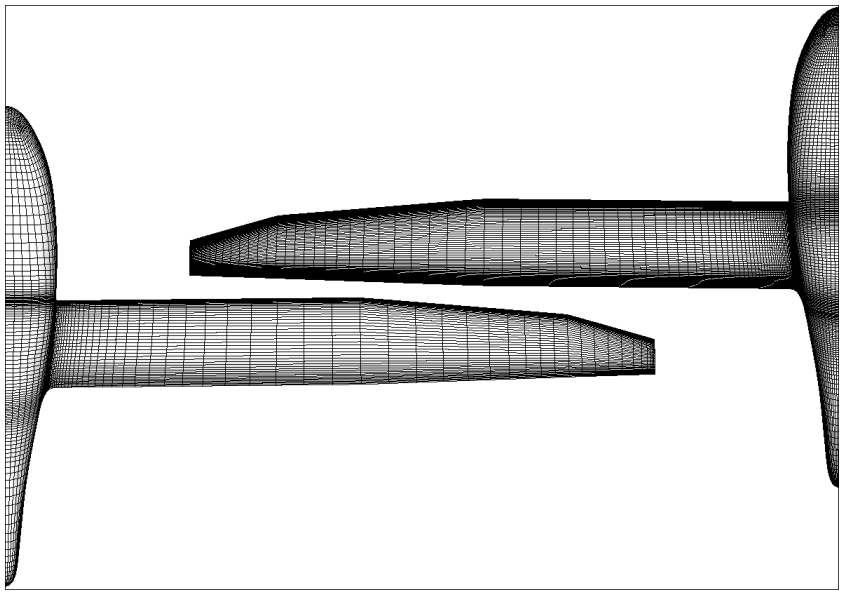

Figure 6. Details of the two surface meshes

With regard to CFD solution set-up, a steady pressure based solver was employed with SIMPLE scheme for pressure-velocity coupling, Least Squares Cell based for Gradient, Standard for Pressure and Second Order Upwind for Momentum and turbulence spatial discretization. As concerns solution computing, a hybrid initialization was applied before the performing the 3000 iterations during which aerodynamic coefficients (optimization objective functions) were monitored and stored.

The cells are clustered on the wall surfaces in order to apply wall functions when using the coarse one and to solve the boundary layer up to the wall when using the fine grid. The wall cells dimension growth rate is in the order of 1.2 in both grids. The Figure 7 reports the wall Y+ distribution for both CFD solutions.

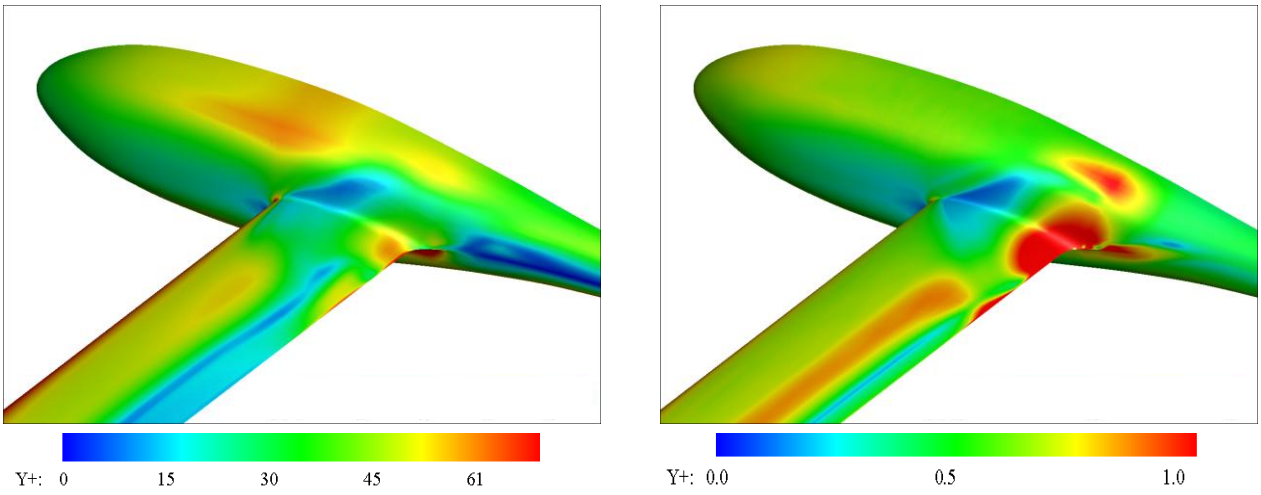

Figure 7. Wall Y+ distribution for the coarse (left) and the fine (right) grid

The regions of the model in the baseline configuration experiencing flow detachment are shown in Figure 8 through the visualization of the streamlines superposed on skin friction coefficient distribution. As visible, the physical phenomenon registered during the experimental flight is numerically reproduced and confirmed by both numerical models although the extent of separation is overestimated using the coarse grid. Therefore, the direct expected impact of this disagreement is the overestimation of the drag and the underestimation of the lift respect to the finer model.

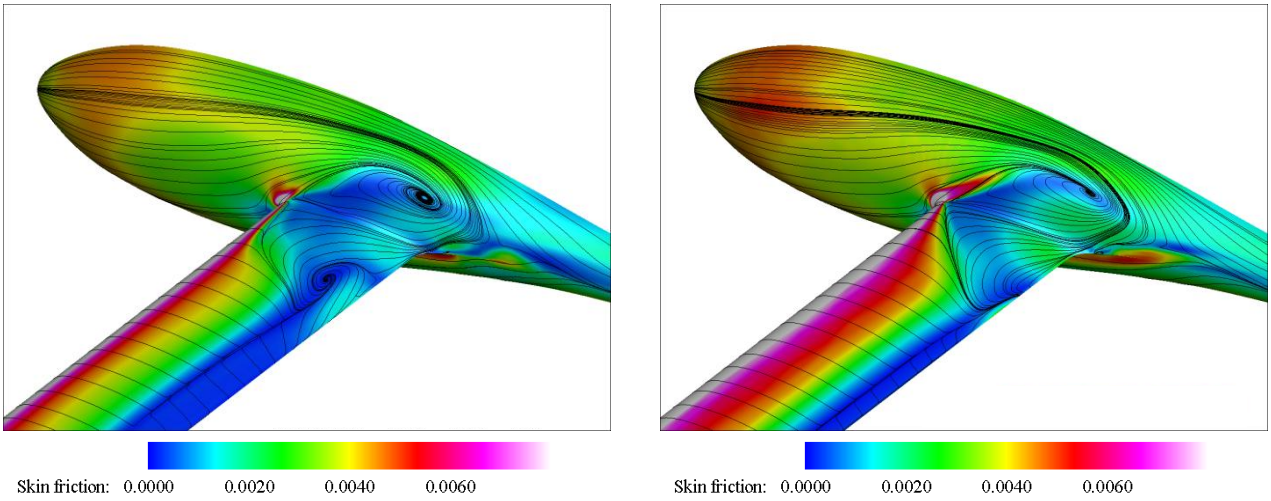

Figure 8. Streamlines superposed on skin friction coefficient distribution for baseline configurations for the coarse (left) and the fine (right) grid

In Figure 9 pressure coefficient profile at different sections of the wing for both the coarse and fine model in the baseline configuration are plotted. In particular, the sections of interest are those having coordinates η (y/c) respectively equal to 0, 2.5, 5, 7.5 and 10%. The separated region and its spanwise extent is also clearly evidenced by the pressure plateau evolution.

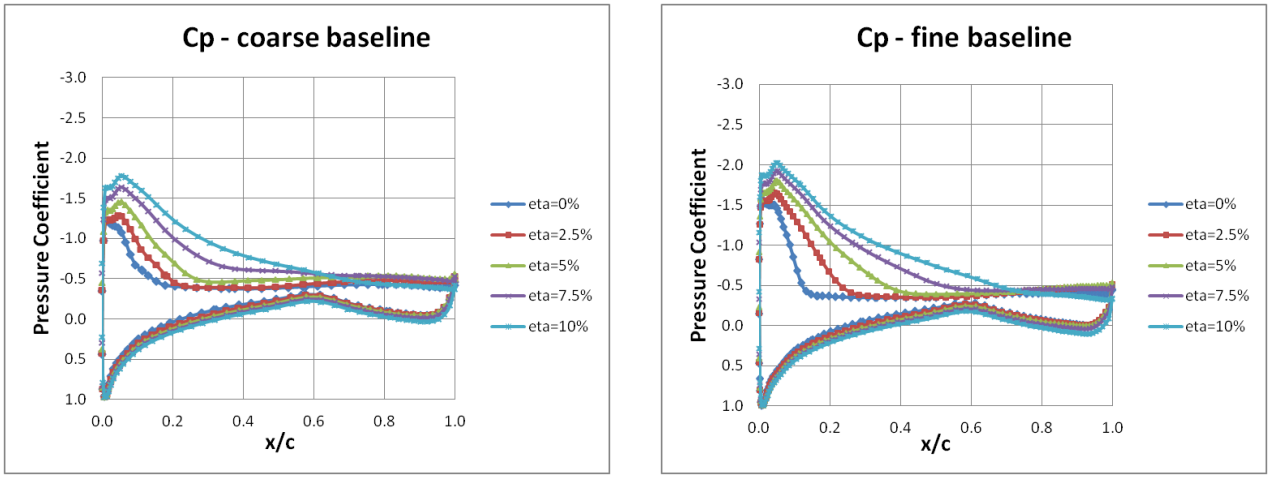

Figure 9. Pressure coefficient profiles along wing sections for baseline configurations

In Table 1 the main results related to aerodynamic coefficients of the baseline configurations are summarized.

Table 1. Main results related to aerodynamic coefficients of the baseline configurations

Parameter	Coarse	Fine
C_d	0.081	0.076
C_l	1.018	1.131
Aerodynamic efficiency	12.56	14.88

The underestimation of the aerodynamic efficiency by the coarse configuration, due to the separation overestimation, is numerically confirmed.

4.2 RBF solutions generation

Considering the CFD results obtained for the baseline configuration, two shape modifications acting on the wing-fuselage junction, respectively nearby the leading edge and trailing edge, were set up. The shape modifier, that is the mathematical framework enabling RBF solutions' computing, for both modifications was generated utilizing the Surfs and Encaps features of RBF Morph [R11]. In particular, one surf set to fix the nodes that are required not to change their position, one cylinder-shaped moving encap to deform the glider's surfaces and one a box-shaped domain encap to limit the action of morphing were employed for each shape modification. The location of the source nodes generated by the described set-up is shown in Figure 4, whilst the effect produced on the surface mesh of the coarse grid by the application of the generated solutions is shown in Figure 10 and Figure 11 respectively.

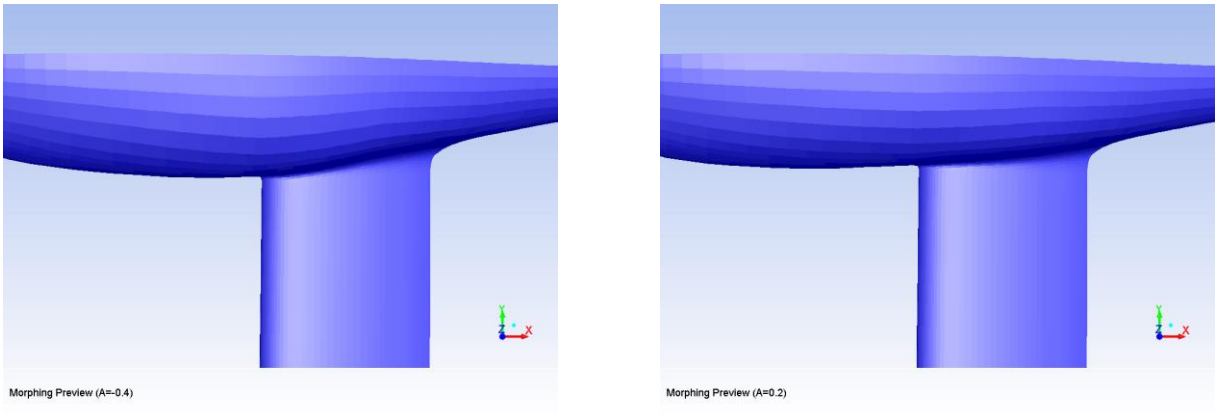

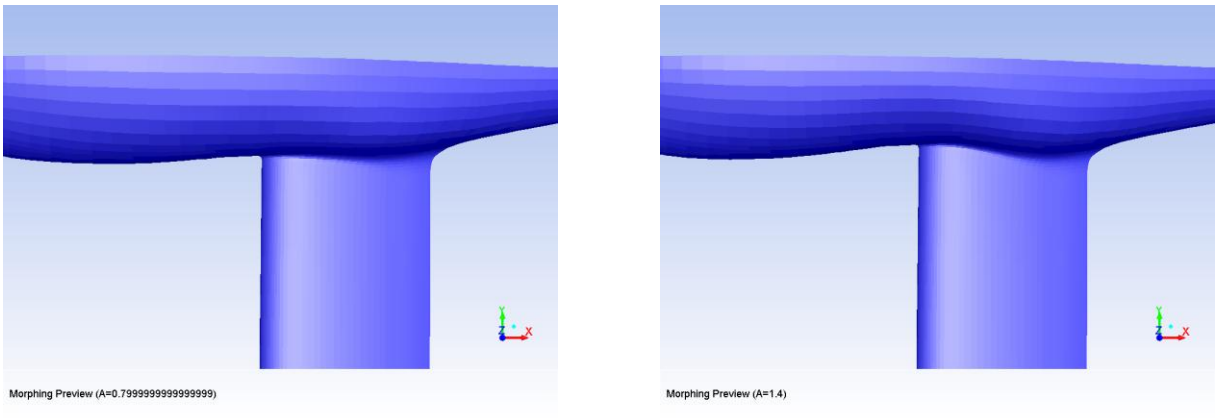

Figure 10. Shape deformation induced by the first shape modifier

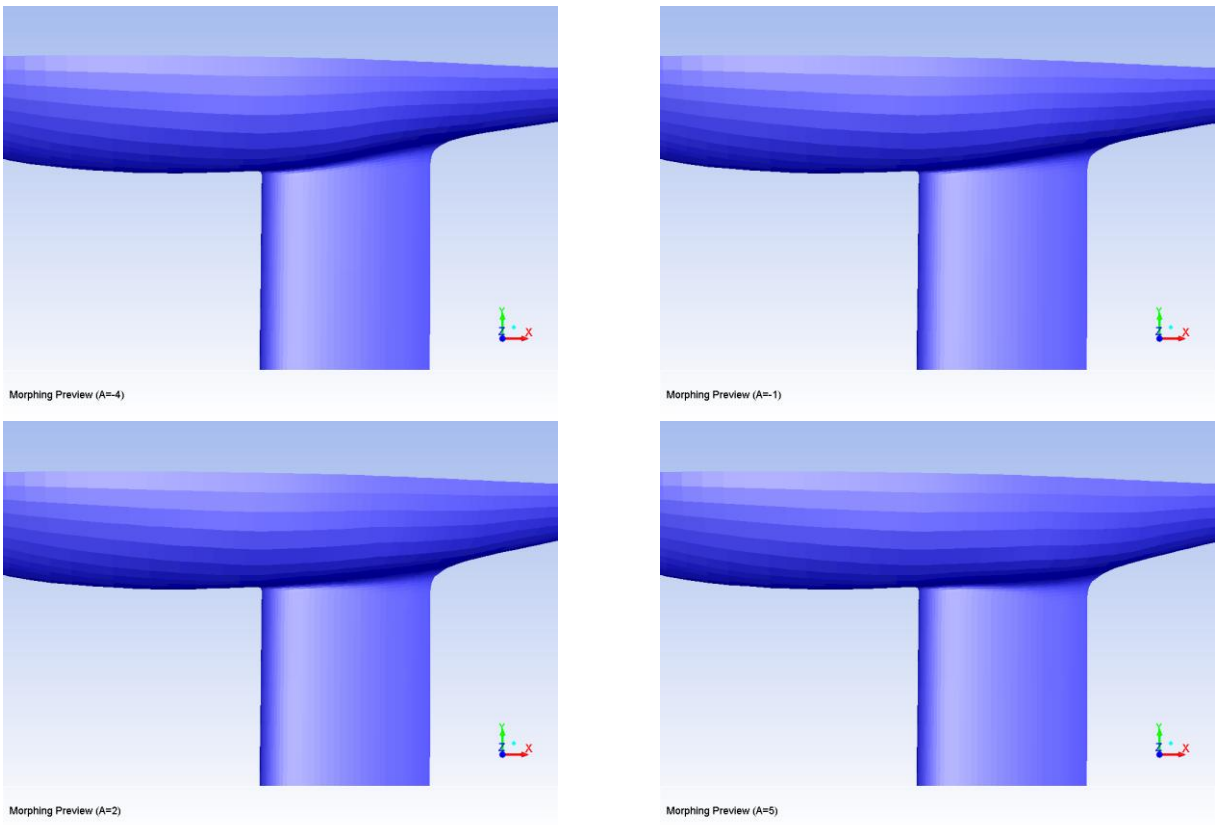

Figure 11. Shape deformation induced by the second shape modifier

According to the best practice suggested for RBF mesh morphing set-up **Error! Reference source not found.**, the range of variation of both modifiers was determined taking into account for detrimental effects on mesh quality.

5 Optimization study results

Once both CFD models and RBF solutions for both shape modifiers were calculated and stored, a DoE campaign was set-up and tuned by DX using the coarse mesh. Through such a model the optimal point is selected using the coarse mesh and, to complete workflow, the fine model is used just two times (baseline & optimal) to verify the performances of achieved shape. In the present study, due to HPC resource limitation, the standard industrial workflow has not be pursued, but will be subject of future investigations.

Imposing a [-0.4;1.4] bound for the amplification of the RBF solution acting near the leading edge, defined input parameter 1 (P1), a [-4;5] bound for the trailing edge one, defined input parameter 2 (P2), the aerodynamic coefficients (C_d=P3 and C_l=P4) and efficiency (P5) as output parameters, the DoE table was populated with 20 DPs, hereinafter referred to as 20-DP, using a Latin hypercube sampling design method. Moreover, in view of accelerating the DoE calculation, all DPs were initialized with the already achieved baseline flow field and then morphed according to the imposed input parameters, obtaining a fully developed and numerically converged CFD solution for each.

The efficiency calculated for each DP using drag and lift coefficients obtained with Fluent is shown in Figure 12.

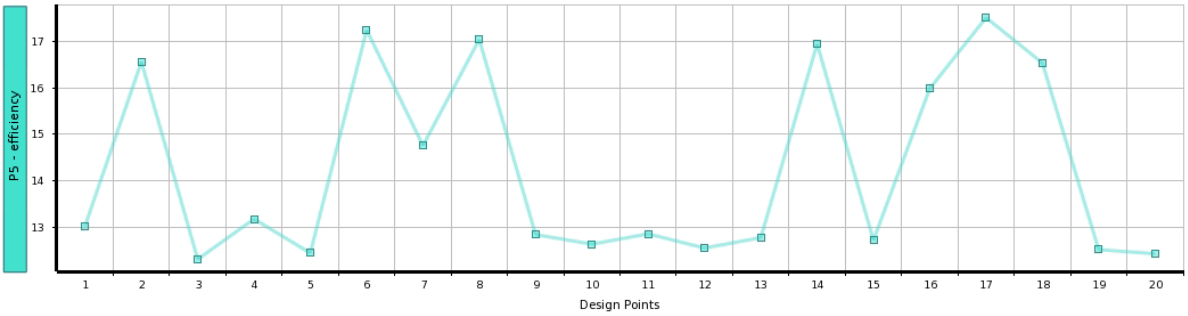

Figure 12. Design points versus aerodynamic efficiency for the 20-DP DoE study

The response surface (RS) dealing with the aerodynamic efficiency, calculated using a Kriging method with variable kernel, and the local sensitivities of objective functions (Output-Parameters) are respectively depicted on the left and right side of Figure 13.

Referring to the RS, even if its regular shape evidences the high significance for the goodness of fit, the portion characterized by the highest value for the efficiency, namely that most interesting from the aerodynamic point of view, turns out to be the result of mathematical approximation since the Latin hypercube method, used to populate the DoE table, does not necessarily cover the extremes (the corners of the design space).

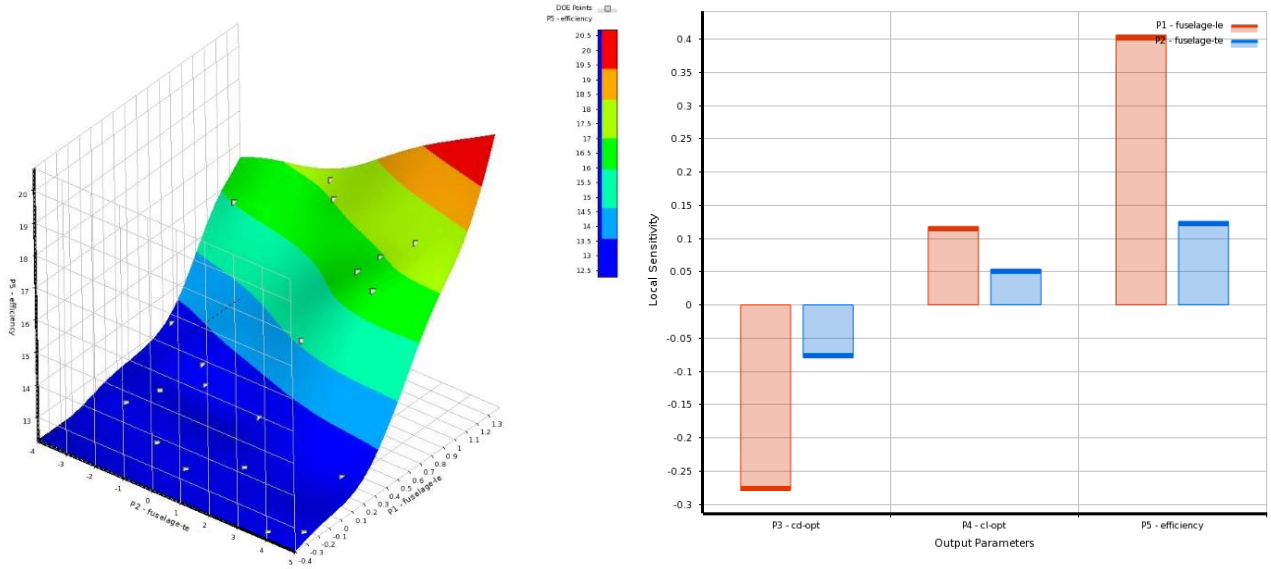

Figure 13. Response surface (left side) and local sensitivity for the 20-DP DoE study (right side)

Relating to local sensitivity sensitivities diagram, the trailing edge shape modifier (P2) has no effects if leading separation occurs. When the leading edge parameters (P1) acts on the fuselage, preventing the leading edge stall, the trailing edge parameters begins to be effective reducing the adverse pressure gradient (and the trailing edge separation). This view explains the higher sensitivity to the P1 parameter.

That being so, considering the judgements just expressed, the original 20-DP DoE was enriched with 5 DPs imposed on the border (P1=1.4) in order to update the RS with a better refinement in the most interesting area achieving the updated RS that is depicted in Figure 14.

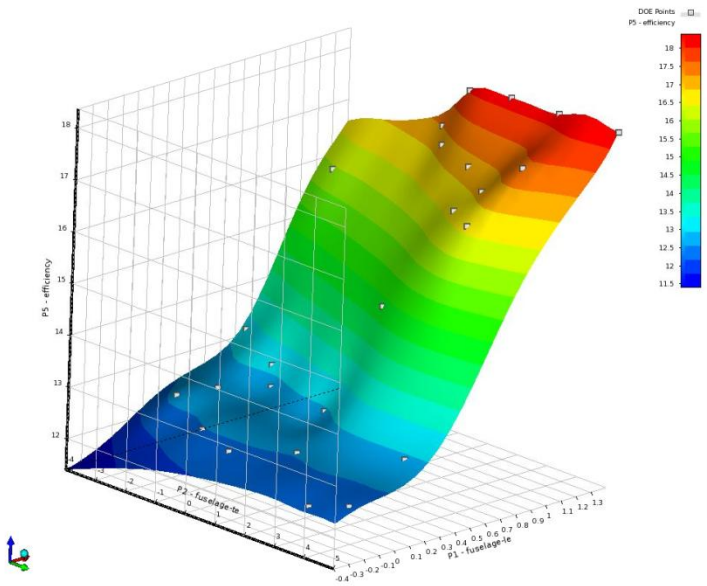

Figure 14 Response surface for the enriched DoE

As visible, although the upper design space border slightly changes its shape, it remains the highest efficiency portion of the RS highlighting a direct correlation between leading edge modifier (P1) and efficiency without global maximum inside the domain. As such, design constraints were imposed to identify the optimal candidates and, accordingly, the amplification of the RBF solution of the first modifier was restricted in order to obtain a maximum displacement of 10 cm. Figure 15 shows the profiles obtained by intersecting the RS with different cutting planes parallel to the P1-P5 plane superposed to the new amplification bound for P1.

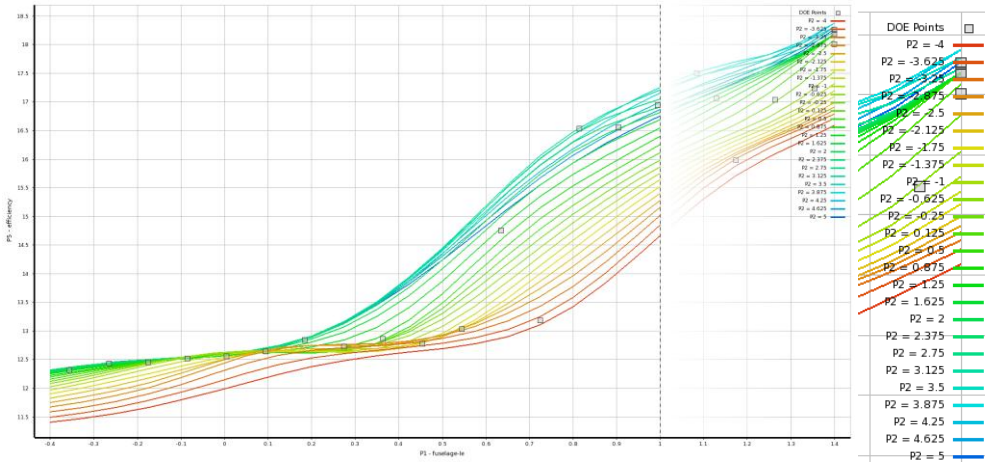

Figure 15 Design constraints for the leading edge modifier

To extract the optimal candidates from the enriched RS, a multi-objective genetic algorithm (MOGA) was used and the corresponding results are shown in Figure 16.

Name	P1 - fuselage-le	P2 - fuselage-te	P3 - cd-opt	P4 - cl-opt	P5 - efficiency	
					Parameter Value	Variation from Reference
Candidate Point 1	0.99547	1.997	0.065132	1.0938	★★ 16.794	0.13 %
Candidate Point 2	0.99349	1.9489	0.06518	1.0934	★★ 16.775	0.01 %
Candidate Point 3	0.99824	1.8974	0.065184	1.0933	★★ 16.773	0.00 %

Figure 16 Candidate points for the RS

Taking into account the sensitivity of the shape variation acting on the trailing edge and its geometrical influence, the Candidate Point 3 was selected as optimal point.

5.1 Optimal candidate verification and optimal CAD export

Applying the combination for the amplification values defined by the Candidate Point 3, a CFD run was performed to quantify the exact values of the objective functions. In Figure 17 the optimal configuration outputs are reported according to what done in Figure 8 for the baseline configuration.

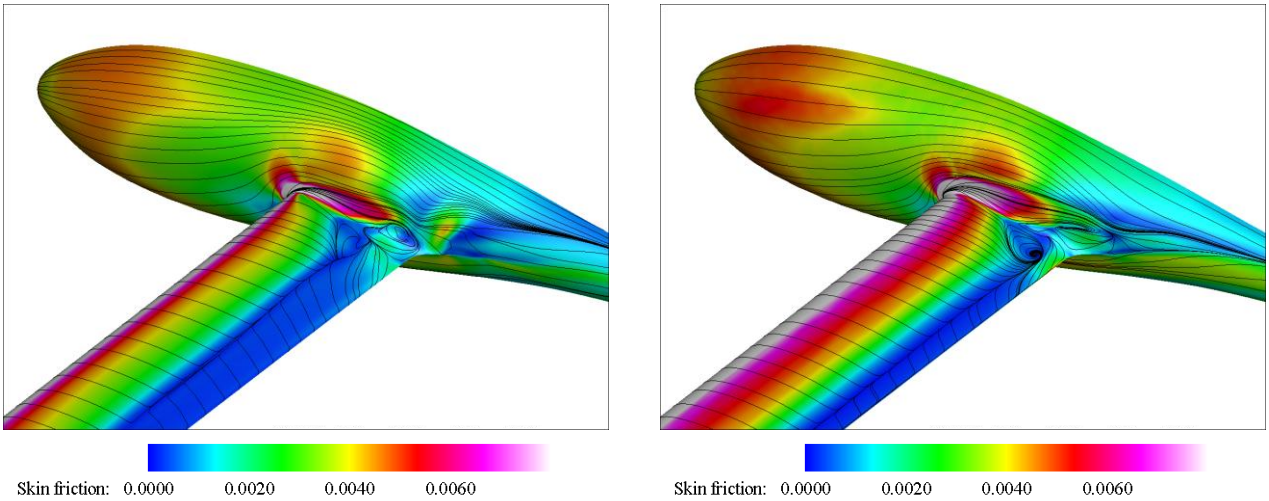

Figure 17. Streamlines superposed on skin friction coefficient distribution for optimal configurations for the coarse (left) and the fine (right) grid

The significant reduction of separation obtained on the optimized solution respect to the baseline geometry is evident. Moreover, the coarse configuration tendency to overestimate the separation is confirmed as well.

The profile of the pressure coefficient at the same sections of the wing already supplied for both the coarse and fine model in the optimal configuration are reported in Figure 18. The reduced separation and the lift increase is also clear from this plots if compared with the pressure distribution obtained on the baseline configuration (Figure 9).

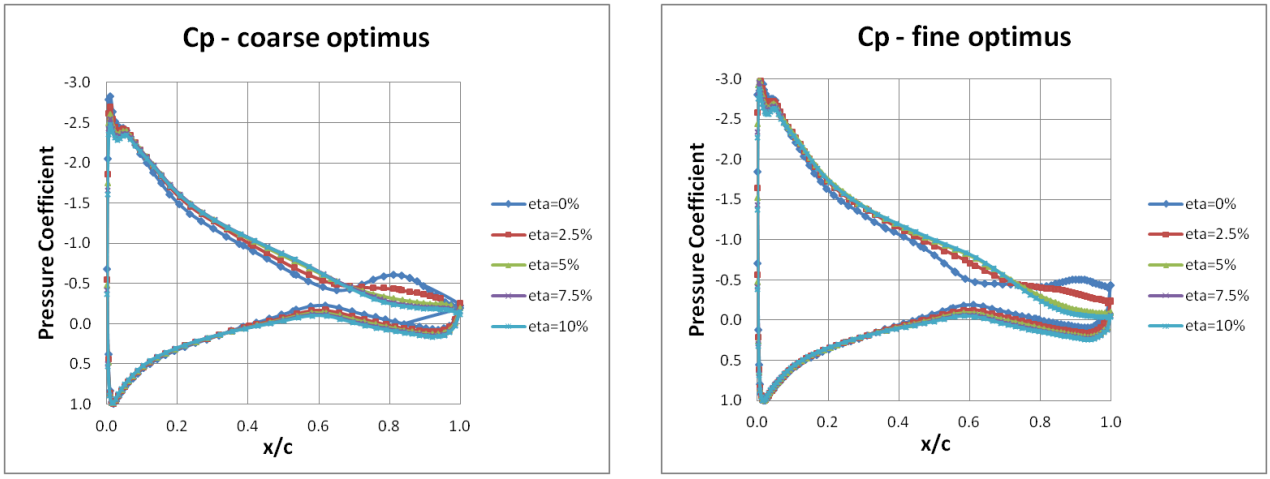

Figure 18. Pressure coefficient profiles along wing monitoring sections for optimal configurations

In Table 2 the main results related to aerodynamic coefficients obtained for the morphed optimal models of the glider are summarized. Such data evidence the achievement of the objectives of the present work. As a matter of fact, firstly the aerodynamic efficiency of the optimal configuration is relevantly improved (33.93%). Secondly, since the aerodynamic efficiency relative variation percentage is almost maintained for the coarse and fine optimal model (33.51% and 33.93% respectively), both the qualitative and quantitative coherency of the numerical behaviour of the coarse and fine model is positively verified and, consequently, the reliability of the adopted resolution strategy is successfully confirmed.

Table 2. Main results related to aerodynamic coefficients

Parameter	Coarse	Fine
C_d	0.065	0.061
C_l	1.093	1.216
Aerodynamic efficiency	16.77	19.93
Efficiency relative variation	33.51%	33.93%

To finalize the proposed numerical optimization approach, the CAD of the optimized configuration, shown in Figure 19, was obtained using the back2CAD feature of the RBF Morph.

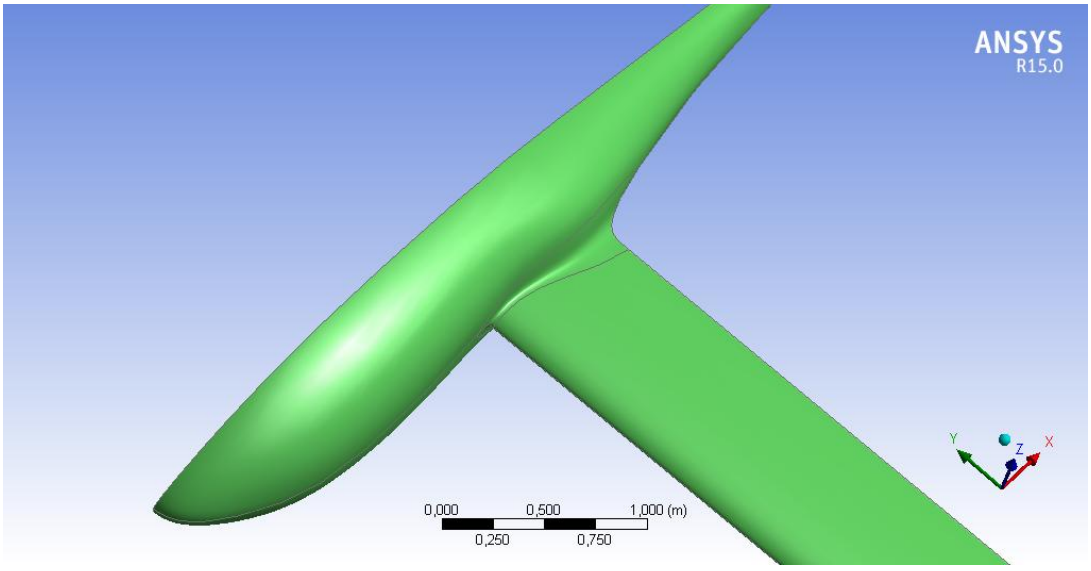

Figure 19. CAD model of the optimized configuration

As previously outlined, to achieve such result the starting CAD the geometry in STEP format was morphed applying the combination of amplification values defined by the Candidate Point 3.

6 Conclusions

In this paper a numerical procedure to enhance the aerodynamic efficiency of an industrial glider was described. Such a procedure is completely manageable in WB environment, it is based on the DoE approach and a mesh morphing technique which allows to save lots of time because it makes use just of the computational model of the baseline configuration. In fact, all the explored variations are generated at run time thanks to the parametric nature of the method.

A relevant improvement in terms of reduction of the separation region and enhancement of aerodynamic efficiency was obtained in agreement with manufacturing constraints. The employed resolution strategy adopts, at first, a low-demanding computational CFD model to carry out the DoE optimization analysis and, then, a more accurate one to verify the obtained optimal solution.

It is worth to notice how the simplified workflow, affordable even with a small sized HPC facility, allows to get an optimal shape which demonstrates a substantial improvement. The increasing of efficiency, as computed by the high fidelity mesh, is close to 34%.

7 Acknowledgments

This work was financially supported by the RBF4AERO Project, funded in part by the European Union 7th Framework Programme (FP7-AAT, 2007 - 2013) under Grant Agreement no. 605396. To get further information, please visit the RBF4AERO's website at www.rbf4aero.eu.

8 References

[R1] RBF4AERO Project, "Innovative benchmark technology for aircraft engineering design and efficient design phase optimisation", 2013.

[R2] Sovani, S., and Khondge, A., "Scaling New Heights in Aerodynamics Optimization: The 50:50:50 Method", White paper available on ANSYS Inc. Website, 2012.

[R3] Caridi, D., and Wade, A., "Higher-Speed CFD", *Professional Motorsport World Magazine*, April-June 2012.

[R4] Petrone, G., Hill, C., and Biancolini, M.E, "Track by Track Robust Optimization of a F1 Front Wing using Adjoint Solutions and Radial Basis Functions", *44th AIAA Fluid Dynamics Conference*, AIAA-2014-3174, 2014

[R5] Biancolini, M.E., Viola, I.M., and M. Riotte, "Sails trim optimisation using CFD and RBF mesh morphing", Computers and Fluids, Elsevier, Volume 93, 10 April 2014, Pages 46–60. DOI: 10.1016/j.compfluid.2014.01.007.

[R6] Biancolini M.E., Ponzini, R., Antiga, l., and Morbiducci, U., "A new workflow for patient specific image-based hemodynamics: parametric study of the carotid bifurcation", Summer School held by CILEA, Conference CompIMAGE 2012, 2012.

[R7] Biancolini, M.E., Travostino, G., and Mancini, M., "Shaping up – Mesh morphing reduces the time required to optimize an aircraft wing", ANSYS Advantage Magazine - Volume VII, Issue 1, 2013.

[R8] Biancolini, M.E., and Groth, C., "An Efficient Approach to Simulating Ice Accretion on 2D and 3D Airfoils", *Advanced Aero Concepts, Design and Operations*, 2014.

[R9] Cella, U., and Biancolini, M. E., "Aeroelastic Analysis of Aircraft Wi*nd-Tunnel Model Coupling Structural and Fluid* Dynamic Codes", *Journal of Aircraft*, Vol. 49, No. 2 (2012), pp. 407-414.

[R10] Reina, G.P., Della Sala, A., Biancolini, M.E., Groth, G., and Caridi D. "Store Separation: Theoretical Investigation of Wing Aeroelastic Response", 4th Aircraft Structural Design Conference, 2014.

[R11] Biancolini M.E., "Mesh Morphing and Smoothing by Means of Radial Basis Functions (RBF): A Practical Example Using Fluent and RBF Morph", *Handbook of Research on Computational Science and Engineering: Theory and Practice*, edited by J. Leng and Wes Sharrock, 2012, pp. 347-380. DOI: 10.4018/978-1-61350-116-0.ch015.

[R12] RBF Morph, "RBF Morph - Users Guide", 2014.